# Optical and current transport properties of CuO/ZnO nanocoral p-n heterostructure hydrothermally synthesized at low temperature

A Zainelabdin, Siama Zaman, Gul Amin, Omer Nur and Magnus Willander

# **Linköping University Post Print**

N.B.: When citing this work, cite the original article.

The original publication is available at www.springerlink.com:

A Zainelabdin, Siama Zaman, Gul Amin, Omer Nur and Magnus Willander, Optical and current transport properties of CuO/ZnO nanocoral p-n heterostructure hydrothermally synthesized at low temperature, 2012, Applied Physics A: Materials Science & Eamp; Processing, (108), 4, 921-928.

http://dx.doi.org/10.1007/s00339-012-6995-2

Copyright: Springer Verlag (Germany)

http://www.springerlink.com/?MUD=MP

Postprint available at: Linköping University Electronic Press http://urn.kb.se/resolve?urn=urn:nbn:se:liu:diva-81220 Optical and current transport properties of CuO/ZnO nanocorals p-n heterostructure

hydrothermally synthesized at low temperature

A. Zainelabdin\*, S. Zaman, G. Amin, O. Nur, and M. Willander

Department of Science and Technology, Linköping University, SE-601 74 Norrköping,

Sweden, Fax: - (+) 461136 327 0

Abstract

We demonstrate the synthesis, and investigate the electrical and optical characteristics of

"nanocorals" (NCs) composed of CuO/ZnO grown at low temperature through the hydrothermal

approach. High density CuO nanostructures (NSs) were selectively grown on ZnO nanorods

(NRs). The synthesized NCs were used to fabricate p-n heterojunctions that were investigated by

the current density-voltage (J-V) and the capacitance-voltage (C-V) techniques. It was found that

the NCs heterojunctions exhibit a well-defined diode behavior with a threshold voltage of about

1.54 V and relatively high rectification factor of ~ 760. The detailed forward J-V characteristics

revealed that the current transport is controlled by an ohmic behavior for V < 0.15 V, whereas at

moderate voltages  $1.46 \le V < 1.5$  the current follows J  $\alpha$  exp ( $\beta V$ ) relationship. At higher

voltages ( $\geq 1.5 \text{ V}$ ) the current follows the relation J  $\alpha \text{ V}^2$ , indicating that the space-charge-limited

current mechanism is the dominant current transport. The C-V measurement indicated that the

NCs diode has an abrupt junction. The grown CuO/ZnO NCs exhibited broad light absorption

range that is covering the UV and the entire visible part of the spectrum.

**Keywords:** CuO, ZnO, nanocorals heterojunction, current- voltage characteristics, absorption

spectrum.

Corresponding author email: <a href="mailto:ahmza@itn.liu.se">ahmza@itn.liu.se</a>

1

#### 1 Introduction

Fabrication of semiconductor devices from their basic building blocks into more complex structures applying the bottom up approach has intensified the global research activities in the last decades. Metal oxides nanostructures (NSs) in particular, are synthesized into very complex structures ranging from nanoparticles to hyper-branched NSs using both low and high temperature growth methodologies [1, 2]. The increased complexity of NSs combined with their relatively high surface area to volume ratio provide excellent chemical, optical, and electrical properties that can be tailored to fabricate future intelligent nano-systems. However, fundamental understanding of the electro-optical properties of these NSs and their fabricated nano-devices is important for developing new applications.

As n-type metal oxide semiconductor, zinc oxide (ZnO) has attracted intensive research attention owing to its diverse interesting properties such as electro-optical, piezoelectric, and magnetic properties [3-6]. With a direct wide band gap (3.37 eV) and relatively large exciton binding energy of (60 meV) ZnO has been widely investigated for many optoelectronic, chemical and bio sensing applications [7-9]. ZnO on the other hand offers the most diverse family of NSs compared to any other metal oxide material known today. To obtain ZnO NSs there are easy synthetic routes at low and high temperatures [10, 11]. The possibility to use relatively low growth temperature (< 100 °C) is enabling the fabrication of these new nano-devices on soft substrates, e.g. on paper as we demonstrated recently [12].

Likewise, cupric oxide (CuO) is another metal oxide material that has been substantially explored for various fields of applications. As a p-type semiconductor having a narrow band gap of (1.35 eV), CuO has great potential as a field emitter, catalyst and as a gas-

sensing medium [13-15]. The physiochemical properties of CuO such as the photoconductivity and the photochemistry can be tailored for fabricating optical switches and solar cells [16]. Different CuO NSs with diverse morphologies were grown using various methods ranging from nanoparticles (NPs) to complex dandelion-shaped hollow structures [17-20]. However, CuO NSs grown through these methods were limitedly applied to the growth of CuO nanopowders since they demonstrated poor adhesion to substrates in general [21]. This will limit CuO NSs functionality for electronic applications due to the lack of intimate junction.

The heterojunction of these two important metal oxides CuO/ZnO was studied for junctions obtained by either mechanical compression or by sputtering procedure, and the samples were further used as gas sensors [22-26]. Although heterojunctions of CuO/ZnO obtained using these procedures exhibited rectifying characteristics they have been assembled in a rather primitive way as mentioned above, e.g. using mechanical compression of ZnO on CuO polycrystalline pellets. So far no reports on CuO/ZnO heterojunctions that were achieved by direct growth of CuO NSs on ZnO NRs have been demonstrated. Recently, few attempts of growing CuO/ZnO composites were performed [27-30]. For these composites either high temperature or expensive UV growth procedures were used. In general the structural, optical, and photovoltaic results presented in these studies suggest that this composite carries great potential for different device applications.

Here, we report the fabrication and characterization of CuO/ZnO nanocorals (NCs) p-n heterojunction on ITO substrate at low temperature of 60 °C. The CuO NSs were specifically assembled on ZnO nanorods (NRs). Therefore, we have successfully overcome both the poor reproducibility of mechanical contacts and solved the substrate adhesion problem of CuO nanomaterial. Moreover, the synthesized NCs revealed broad light absorption that is covering the

UV-Vis-NIR range of the spectrum. The fabricated NCs p-n diode exhibited excellent electrical characteristics with obvious rectifying behavior that may be used to construct solar cells, photodetectors and gas sensors.

### 2 Experimental

The fabrication of CuO/ZnO NCs based p-n diode started by growth using two step hydrothermal procedures. In the first procedure well aligned ZnO NRs were grown as reported recently [11]. In short, ZnO NPs solution prepared by modifying the procedure described by Pacholiski et al. [31] was deposited on an ITO substrate by spin coating process. The pre-coated substrate was immersed in an equimolar 50 mM solution containing [Zn (NO<sub>3</sub>)<sub>2</sub>.6 H<sub>2</sub>O] and [C<sub>6</sub>H<sub>12</sub>N<sub>4</sub>. HMT] held at 50 °C for 6-8 h. After the reaction was completed the substrate was thoroughly rinsed in DI-water under low sonication power and then dried at room temperature. This process has resulted in the growth of dense ZnO NRs. After ZnO NRs growth, a polystyrene (PS) was used as an insulating material between individual NRs, this was then followed by reactive ion etching (RIE) to uncover 2/3 of the NRs for the subsequent growth of CuO NSs. In the second hydrothermal procedure a 5 mM aqueous solution of [Cu (NO<sub>3</sub>)<sub>2</sub>.3H<sub>2</sub>O] was prepared and the freshly processed ZnO NRs sample was immediately immersed for 4 h and the solution temperature was held at 60 °C. The substrate was then collected and carefully cleaned with DIwater and ethanol. Then the PS was used again to insulate the grown CuO/ZnO NCs from each other followed by RIE to expose the tips of the NCs for the subsequent last metallization step. Finally, the p-n diode was realized by thermally evaporating 100 nm Au contacts through a shadow mask on top of the NCs with an active diodes area of about 0.02 cm<sup>2</sup>. The synthesized NCs were characterized using different techniques including scanning electron microscope (SEM), x-rays diffraction (XRD), transmission electron microscopy (TEM), and UV-Vis-NIR absorption spectroscopy. While the fabricated NCs p-n heterojunction diodes were investigated at room temperature with HP Agilent 4155B semiconductor parameter analyzer and capacitance-voltage measurements.

#### 3 Results and Discussion

Figure 1, shows representative SEM images of the ZnO NRs grown on ITO substrate at 50 °C for 6 h. Figure 1a, clearly displays that ZnO NRs exhibit reasonable vertical alignment perpendicular to the substrate surface. Figure 1b shows a low magnification SEM of CuO/ZnO NCs that were hydrothermally grown for 4 h. A magnified SEM image of the composite NCs can be seen in Fig. 1c. In this figure (Fig. 1c) CuO NSs were adhered to ZnO NRs forming a coral shaped NSs in which ZnO NR is acting as the core. Figure 1d demonstrates a SEM image taken at 40 ° tilt angle viewing highly branched CuO NSs selectively deposited on ZnO NRs. The SEM images of Fig.1c-1d also illustrate that there are apparently physical connections between adjacent NCs. Owing to the interconnection between the adjacent NCs large area nano-devices can be fabricated. Transmission electron microscopy image of CuO/ZnO NCs grown for 1.5 h is presented in Fig. 2a. This TEM image indicates that CuO NSs adhere to ZnO NRs robustly. It was also observed that two or more ZnO NRs can share the same CuO NS to form NCs. The dotted hexagon in the TEM image of Fig. 2a depicts a ZnO NR that was detached during the TEM sample preparation. We have also observed that the grown CuO NSs start to grow first on the lateral sides of ZnO NRs and then tend to cover the NR surface entirely. Detailed TEM measurements (not shown here) revealed that in general there are no crystallographic relations between the two oxide NSs which is in good agreement with previous reports [30]. The XRD pattern of CuO/ZnO NCs exhibits three diffraction peaks as shown in Fig. 2b. The peak at 34.47 ° is corresponding to the (002) direction of the wurtzite structure of ZnO and well agrees with the value available in the (JCPDS card No. 36-1451). On the other hand the additional two peaks at  $2\theta$  values of 35.57 ° and 38.73 ° are corresponding to the ( $\overline{1}$ 11)/(2002) and (111)/(2000) planes of pure monoclinic structure of CuO (JCPDS card No. 05-0661). As clearly visible CuO NSs exhibited a weak and broad XRD peaks which can be ascribed to small CuO nanocrystals that were assembled through the well know oriented attachment process [17-19]. No additional peaks related to other phases such as Cu, Cu(OH)<sub>2</sub> or Cu<sub>2</sub>O were detected suggesting that the grown CuO NSs are of high purity.

The current density-voltage (J-V) characteristics of CuO/ZnO NCs p-n heterojunction diode were studied at room temperature. The results are presented in Fig. 3 in a linear scale together with the schematic diagram of the diode structure (inset). As can be seen the rectifying behavior of the J-V of the NCs heterojunction diode is evident. The threshold voltage (V<sub>th</sub>) of the NCs diode was extracted to be about 1.52 V, a value which agrees closely with the reported value of 1.55 V for sputtered CuO thin film on polycrystalline ZnO substrate [25]. At 3 V reverse bias the leakage current density was as low as 0.225 mA/cm<sup>2</sup> resulting in a forward-toreverse current ratio of about 762. This value is quite acceptable considering the low growth temperature used for these NCs. The NCs heterojunction demonstrates a soft breakdown at about -7 V and some of the diodes show even higher breakdown voltage of up to -15 V (not shown here). The semi-log (J-V) characteristics of the NCs heterojunction diode are presented in Fig. 4a along with the ohmic contact characteristics of both contacts to CuO NSs and ZnO NRs (inset). The ohmic contacts exhibit low specific resistances without performing any annealing steps after the device was fabricated. The contact resistance of Au and ITO to CuO and ZnO were found to be about  $3.2 \times 10^{-3} \Omega$  and  $1.7 \times 10^{-3} \Omega$ , respectively.

The relationship between the current and the applied voltage across the heterojunction can be expressed as [32].

$$I = I_o \left[ exp^{\left(\frac{V - IR_s}{n V_i}\right)} - 1 \right] \tag{1}$$

where the pre-exponential factor  $I_0$  is the reverse saturation current, V is the applied voltage across the junction,  $R_s$  is the series resistance included to account for the deviation of the I-V curve from linearity at high current region,  $V_i = kT/q$  is the thermal voltage, k is Boltzmann constant, T is the absolute temperature, and n is the so-called junction ideality factor. The ideality factor is determined from the slope of the straight line region of the forward bias log I-V characteristics. By using Eq. (1) and Fig. 4a the value of the ideality factor of the NCs heterojunction is about 1.58 at low forward bias  $0.03 - 0.15 \ V$ , and about 6.63 at moderate applied forward bias of  $0.17 - 1.46 \ V$ . The value of the ideality factor deviates largely to 21.3 at high applied forward bias of 1.5- 3 V. This value is indeed too large for fitting the relationship described in Eq. (1). The large deviation of the J-V curve in Fig. 4a at high voltages  $> 1.5 \ V$  suggests that the diode series resistance  $(R_s)$  plays a major role at high forward bias as expected.

By using Eq. (1) and plotting I/(dI/dV) against the current, one attains a linear curve as shown in Fig. 4b. The graph has an intercept of  $(nV_i)$  at I=0 and a slope of  $R_s$ . Consequently, the ideality factor n can also be obtained using Fig. 4b to be 6.80 which in close agreement with the value determined above. The diode series resistance was found to be 369  $\Omega$  and this value is consistent with the experimental curve. The high ideality factor in the present NCs heterojunction diode can be attributed to the large series resistance, defect states existing in the interface of CuO/ZnO and the parasitic rectifying junction within the NCs diode [33]. Figures 5(a) shows the log-log (J–V) characteristics plot at forward bias. It is evident from Fig. 5a that the NCs diode

exhibits three distinct transport regions depending on the applied bias voltage. The current transport in the NCs diode follows a linear dependence at low voltage  $\leq 0.15$  V, i.e. J  $\alpha$  V<sup>1</sup>. This indicates that the current transport in this region is dominated by tunneling at low bias voltages. At intermediate voltages  $0.15 < V \ge 1.46$  V an exponential dependence of the current is evident, where J  $\alpha$  exp ( $\beta$ V) in which  $\beta = 6.16$  V<sup>-1</sup>. The dominant current transport mechanism in this regime is recombination tunneling [34, 35]. Moreover, at high applied voltages > 1.5 V the current–voltage characteristics follow a power law relation i.e. J  $\alpha$  V<sup>2</sup>. The power law relation in this region suggests that the dominating transport mechanism is space–charge limited (SCL) current [34-39]

The capacitance–voltage (C–V) characteristics at a frequency of 1 MHz of CuO/ZnO NCs heterojunction diode was also performed at room temperature. Figure 5b shows the plot of  $C^{-2}$  vs V, in which the maximum applied bias was – 3 V. The inset in this figure shows the C-V curve. A linear relationship between  $C^{-2}$  and V was observed up to – 2.8 V, an indication of an abrupt junction as mentioned above. The intercept of the line at  $C^{-2} = 0$  represents the so-called junction built- in potential  $V_{bi}$ . From the  $C^{-2}$  vs V plot a value of 1.54 V for  $V_{bi}$  is obtained. This value is closely consistent with the  $V_{th}$  obtained from the J–V curve. The  $V_{bi}$  value of 1.54 V obtained in this study is also consistent with the value of 1.55 V obtained for CuO/ZnO thin film heterojunctions reported elsewhere [25].

The measurement of the optical absorption spectrum of a semiconductor material is the most direct and precise way of measuring the fundamental absorption edge and it yields the value of the band gap ( $E_g$ ). The room temperature (RT) optical absorption spectra of ZnO NRs (black curve), as-grown CuO/ZnO NCs (blue curve), and that of CuO/ZnO NCs composite after 1 h heat treatment at 400 °C under O<sub>2</sub> ambiance (red curve) are shown in Fig. 6. The ZnO NRs

absorption spectrum exhibits broad UV band extending from 3.21 eV up to 4.0 eV (not shown) with band edge absorption at ~ 3.32 eV. The obtained value of the band edge of ZnO NRs is consistent with the exciton absorption of ZnO (373 nm) [40]. Furthermore, the absorbance spectrum of ZnO NRs exhibits surplus absorption in the visible part < 3 eV, indicating that large number of defects levels appear in the bandgap of ZnO. The absorbance spectrum of the asgrown CuO/ZnO NCs demonstrated in Fig. 6 reveals very broad absorption covering almost the whole solar spectrum from ~ 1.24 eV to 4.1 eV with considerable absorption in the visible range (Fig. 6). The heat treatment of CuO/ZnO NCs is significantly broadened the absorption band of the NCs composite. This is attributed either to the improvement of the grown NCs crystal quality, and/or due to the formation of an excess defects on the interface of as grown CuO/ZnO NCs.

Finally, on the basis of our experimental results and the available values regarding the band diagrams of ZnO and CuO, a tentative energy band diagram of CuO/ZnO NCs p-n heterojunction can be constructed in accordance with the Anderson model. The obtained band gap  $E_{g\ ZnO}$  of ZnO NRs is ~ 3.32 eV with an energy difference ( $\Delta\epsilon_n$ ) between the conduction band edge and the Fermi level  $E_{Fn}$  ( $\Delta\epsilon_n = E_C - E_F$ ) of ~ 0.05 eV were reported for ZnO [41]. Whereas an electron affinity ( $\chi_{e\ ZnO}$ ) of 4.35 eV was reported for ZnO [42]. The value of the band gap  $E_g$   $\epsilon_{cuO}$  of the CuO is highly controversial issue. Different researches reported different values of the  $\epsilon_{g\ CuO}$  with values ranging from 1.35 eV to 1.8 eV [43-47]. Here, we applied the value of 1.35 eV for the  $\epsilon_{g\ CuO}$  since it is the most reasonable and accepted value. The energy difference  $\epsilon_{g\ CuO}$  between the valence band and the Fermi level  $\epsilon_{g\ CuO}$ , and the electron affinity ( $\epsilon_{g\ CuO}$ ) of CuO were reported to be 0.13 eV, and 4.07 eV, respectively, [43, 44]. From these values the conduction and valence bands discontinuities  $\epsilon_{g\ CuO}$  and  $\epsilon_{g\ CuO}$  are estimated to be  $\epsilon_{g\ CuO}$  and  $\epsilon_{g\ CuO}$  are estimated to be  $\epsilon_{g\ CuO}$  and  $\epsilon_{g\ CuO}$  a

-  $E_{g\ CuO}$ ) -  $\Delta E_{C}$ ] = 1.69 eV, respectively. Based on these values and neglecting the interface states, the constructed band diagram of CuO/ZnO NCs heterojunction is schematically shown in Fig. 7.

The energy band diagram of the synthesized CuO/ZnO NCs p-n diode provides a first order estimation of their heterojunction under thermal equilibrium condition. Nevertheless, the energy band diagram does not take into account the contribution of the interface states, which are verified by the relatively large deviation of the ideality factor determined from the measured J-V curve. The identification of the origin and the influence of the interface states in the CuO/ZnO NCs heterojunction are crucial for future potential device applications.

#### **4 Conclusions**

In summary, a controlled hydrothermal approach was used to synthesis well adhered CuO/ZnO NCs heterojunctions at low temperature. The synthesized NCs were characterized with various techniques, and it is found that CuO NSs exhibit high selectivity to ZnO NRs along with excellent adhesion affinity. The synthesized NCs were utilized to fabricate a p-n heterojunction and were investigated using I-V, C-V measurements and absorption spectroscopy. The NCs heterojunction revealed a typical rectifying behavior with a threshold voltage of 1.54 V and a rectification factor of ~ 760. The forward current transport is limited by three transport mechanisms depending on the applied forward bias. The NCs heterostructure exhibited strong light absorption covering the UV-Vis-NIR range. This study and results presented here emphasize the applicability of CuO/ZnO NCs heterojunctions for the fabrication of efficient, low-cost electronics and optoelectronic nano-devices particularly solar cells, field emitters and sensors devices.

#### References

- 1. O.V. Kharissova and B.I. Kharisov, Ind. Eng. Chem. Res. **49**, 11142 (2010)
- 2. Q. Zhang, S.J. Liu, and S.H. Yu, J. Mater. Chem. 19, 191 (2009)
- 3. S. Ilican, M. Caglar, and Y. Caglar, Appl. Surf. Sci. **256**, 7204 (2010)
- 4. K. Ando, H. Saito, Z.W. Jin, T. Fukumura, M. Kawasaki, Y. Matsumoto, and H. Koinuma, J. Appl. Phys. 89, 7284 (2001)
- 5. P. Sharma, A. Gupta, K.V. Rao, F.J. Owens, R. Sharma, R. Ahuja, J.M.O. Guillen, B. Johansson, and G.A. Gehring, Nature Materials. 2, 673 (2003)
- 6. Z.L. Wang and J.H. Song, Science. **312**, 242 (2006)
- 7. R. Ghosh, S. Fujihara, and D. Basak, Journal of Electronic Materials. 35, 1728 (2006)
- 8. J.Y. Park, D.E. Song, and S.S. Kim, Nanotechnology. 19, 105503 (2008)
- 9. M.H. Asif, A. Fulati, O. Nur, M. Willander, C. Brannmark, P. Stralfors, S.I. Borjesson, and F. Elinder, Appl. Phys. Lett. **95**, 023703 (2009)
- 10. Z.L. Wang, J. Phys.: Condens. Matter. **16**, R829 (2004)
- 11. A. Zainelabdin, S. Zaman, G. Amin, O. Nur, and M. Willander, Cryst. Growth. Des. **10**, 3250 (2010)
- 12. G. Amin, S. Zaman, A. Zainelabdin, O. Nur, and M. Willander, Phys. Status. Solidi-R. 5, 71 (2011)
- 13. Y.W. Zhu and et al., Nanotechnology. **16**, 88 (2005)
- 14. F. Teng, W. Yao, Y. Zheng, Y. Ma, Y. Teng, T. Xu, S. Liang, and Y. Zhu, Sensors and Actuators B: Chemical. 134, 761 (2008)
- X.Y. Xue, L.L. Xing, Y.J. Chen, S.L. Shi, Y.G. Wang, and T.H. Wang, J. Phys. Chem. C.
   112, 12157 (2008)

- M. Abaker, A. Umar, S. Baskoutas, S.H. Kim, and S.W. Hwang, J. Phys. D: Appl. Phys. 44, 155405 (2011)
- 17. H.L. Xu, W.Z. Wang, W. Zhu, L. Zhou, and M.L. Ruan, Cryst. Growth. Des. **7**, 2720 (2007)
- 18. C.H. Lu, L.M. Qi, J.H. Yang, D.Y. Zhang, N.Z. Wu, and J.M. Ma, J. Phys. Chem. B. **108**, 17825 (2004)
- 19. B. Liu and H.C. Zeng, J. Am. Chem. Soc. **126**, 8124 (2004)
- 20. L. Zhu, Y. Chen, Y. Zheng, N. Li, J. Zhao, and Y. Sun, Materials Letters. **64**, 976 (2010)
- D. Li, Y.H. Leung, A.B. Djurisic, Z.T. Liu, M.H. Xie, J. Gao, and W.K. Chan, J. Cryst. Growth. 282, 105 (2005)
- 22. G. Uozumi, M. Miyayama, and H. Yanagida, J. Mater. Sci. **32**, 2991 (1997)
- 23. J.D. Choi and G.M. Choi, Sensors and Actuators B: Chemical. 69, 120 (2000)
- 24. D.H. Yoon, J.H. Yu, and G.M. Choi, Sensors and Actuators B: Chemical. 46, 15 (1998)
- 25. K.K. Baek and H.L. Tuller, Solid State Ionics. **75**, 179 (1995)
- 26. S.J. Jung and H. Yanagida, Sensors and Actuators B: Chemical. 37, 55 (1996)
- 27. S. Mridha and D. Basak, Semicond. Sci. Tech. **21**, 928 (2006)
- 28. Y. Zhu, C.H. Sow, T. Yu, Q. Zhao, P. Li, Z. Shen, D. Yu, and J.T.L. Thong, Adv. Funct.

  Mater. 16, 2415 (2006)
- 29. S. Jung, S. Jeon, and K. Yong, Nanotechnology. **22**, 015606 (2011)
- 30. Z. Guo, X. Chen, J. Li, J.H. Liu, and X.J. Huang, Langmuir. 27, 6193 (2011)
- 31. C. Pacholski, A. Kornowski, and H. Weller, Abstracts of Papers of the American Chemical Society. **224**, U351 (2002)
- D.K. Schroder, Semiconductor material and device characterization, John Wiley, Hoboken,
   N.J., 2005.

- 33. D.C. Kim, W.S. Han, H.K. Cho, B.H. Kong, and H.S. Kim, Appl. Phys. Lett. **91**, 231901 (2007)
- 34. P. Klason, O. Nur, and M. Willander, Nanotechnology. 19, 415708 (2008)
- 35. J.D. Ye, S.L. Gu, S.M. Zhu, W. Liu, S.M. Liu, R. Zhang, Y. Shi, and Y.D. Zheng, Appl. Phys. Lett. 88, 182112 (2006)
- 36. N.K. Reddy, Q. Ahsanulhaq, J.H. Kim, and Y.B. Hahn, Appl. Phys. Lett. 92, 043127 (2008)
- 37. J.A. Edmond, K. Das, and R.F. Davis, J. Appl. Phys. **63**, 922 (1988)
- 38. R.L. Hoffman, J.F. Wager, M.K. Jayaraj, and J. Tate, J. Appl. Phys. **90**, 5763 (2001)
- 39. M.A. Lampert and P. Mark, Current injection in solids, Academic Press Inc, New York, 1970.
- 40. M. Haase, H. Weller, and A. Henglein, J. Phys. Chem-Us. **92**, 482 (1988)
- 41. P.S. Nayar, J. Appl. Phys. **53**, 1069 (1982)
- 42. Z. Guo, D.X. Zhao, Y.C. Liu, D.Z. Shen, J.Y. Zhang, and B.H. Li, Appl. Phys. Lett. **93**, 163501 (2008)
- 43. F.P. Koffyberg and F.A. Benko, J. Appl. Phys. **53**, 1173 (1982)
- 44. M.T.S. Nair, L. Guerrero, O.L. Arenas, and P.K. Nair, Appl. Surf. Sci. **150**, 143 (1999)
- 45. S.C. Ray, Sol. Energ. Mat. Sol. C. **68**, 307 (2001)
- 46. F. Marabelli, G.B. Parravicini, and F. Salghettidrioli, Phys. Rev. B. **52**, 1433 (1995)
- 47. R.V. Pisarev, V.V. Pavlov, A.M. Kalashnikova, and A.S. Moskvin, Phys. Rev. B. 82, 224502 (2010)

## **Figures caption**

# Figure 1

SEM images of (a) hydrothermally grown ZnO NRs at 50 °C on ITO substrate, (b) low magnification SEM image of CuO/ZnO NCs hydrothermally grown at 60 °C, (c) a high magnification SEM of the NCs shown in (b), and (d) 40 ° tilted SEM image of the CuO/ZnO NCs.

#### Figure 2

TEM image of CuO/ZnO NSs hydrothermally grown for 1.5 h showing that two or more ZnO NRs can share the same CuO NS, the dotted hexagon denoting a missing NR (a), and the XRD pattern of the CuO/ZnO NCs hydrothermally grown at  $60 \, {}_{\circ}$ C (b).

## Figure 3

Current density-voltage characteristics of the CuO/ZnO NCs heterojunction diode, the inset is the schematic diagram of the diode.

## Figure 4

The semilog current density-voltage characteristics of the CuO/ZnO NCs heterojunction (a) , the inset shows the ohmic contact characteristics of the Au and ITO, and (b) I/(dI/dV) vs current curve of the NCs heterojunction diode.

**Figure 5**(a) the forward-bias log (J)-log (V) characteristics of CuO/ZnO NCs heterojunction, (b) The capacitance- voltage (C<sup>-2</sup>- V) characteristics of the CuO/ZnO NCs heterojunction, inset is the C-V curve.

# Figure 6

The absorption spectra of ZnO NRs, as-grown CuO/ZnO NCs, and CuO/ZnO NCs annealed for 1 h under O2 flow at  $400\,^{\circ}$ C.

# Figure 7

The constructed energy band diagram of the CuO/ZnO NCs heterojunction under thermal equilibrium conditions.

Figure 1

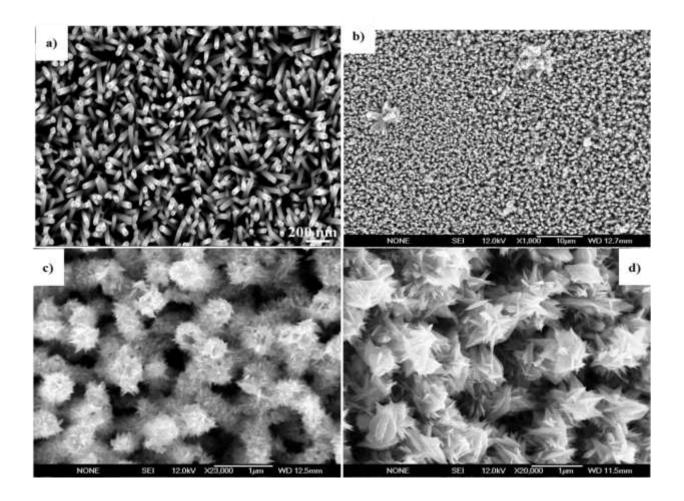


Figure 2

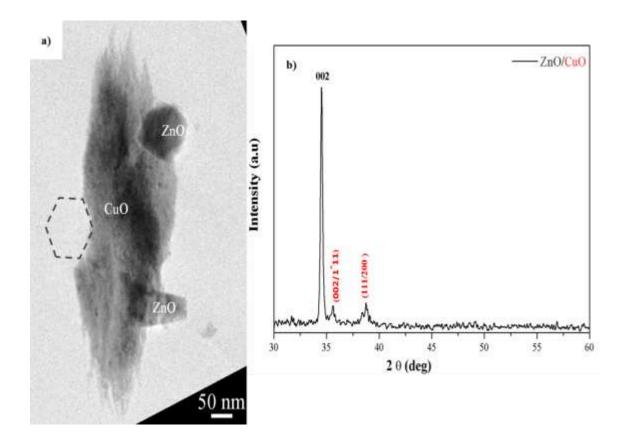


Figure 3

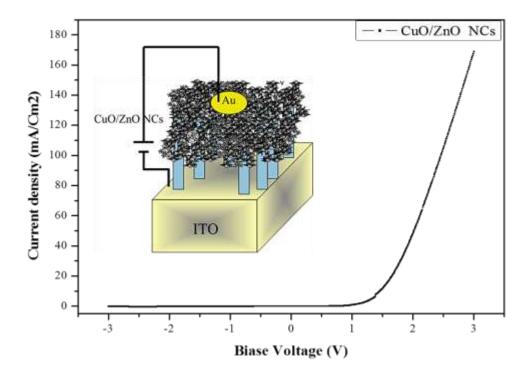


Figure 4

Fig. 4(a)

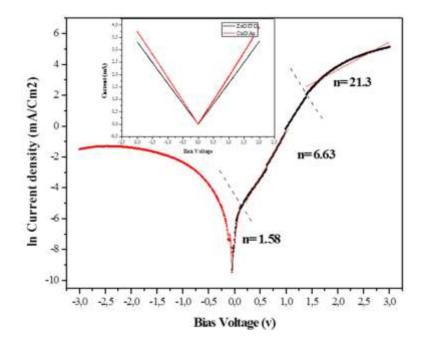


Fig. 4 (b)

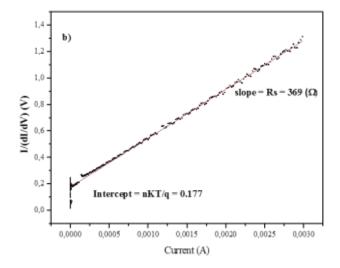


Figure 5

Fig. 5 (a)

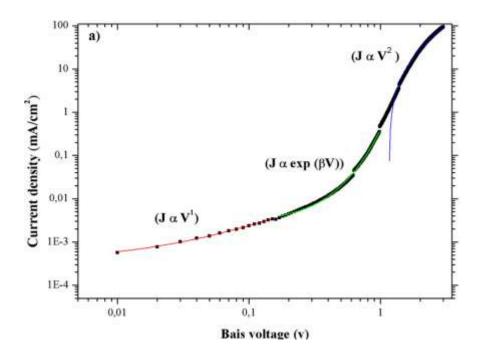


Fig. 5 (b)

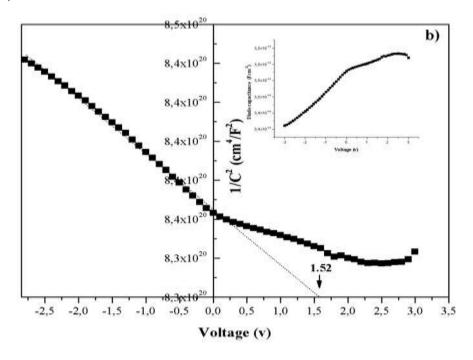


Figure 6

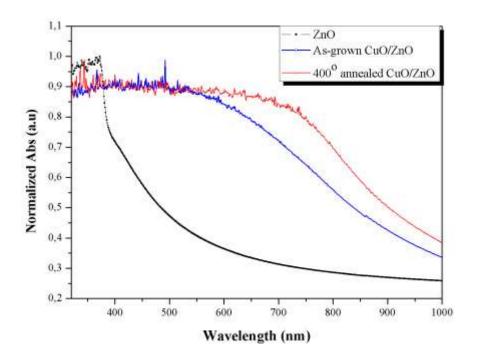


Figure 7

